Identification and validation of novel MAP kinase substrates and interactors

1. Background

Mitogen activated protein kinases (MAPKs) have been identified as fundamental regulators of several critical biological processes like control of cell proliferation and cell death however – except a handful number of known effectors – the precise molecular elements connecting MAPK-driven actions to the genomic level are poorly understood. While MAPK-activated canonical transcription factors are widely used to explain MAPK-dependent signaling recent understanding indicates a more complex role for MAPKs via regulation chromatin state also modulating gene regulator region accessibility for other elements of the transcription. Therefore, it is fundamental to focus on these novel aspects of MAPK regulatory role by identifying non-classical effectors and modulators connected to gene regulation. Since their broad range of action, it is difficult to dissect individual MAPK-dependent functions. As the part of this we approached this question from two directions: on one hand we aimed to extend the MAPK interactome toward less obvious targets and proteins facilitating MAPK-dependent phosphorylation while also applying a reversed strategy via reconstruction of the effector cascade responsible for executing genomic effects of MAPKs.

2. Results

1.1. Validation of predicted novel interaction partners

In order to extend MAPK interaction network MAPPIT (mammalian protein-protein interaction trap) high-throughput screen has been previously performed with ERK2, p38α and JNK1 as baits against human protein expression library to identify candidates [1]. This method is based on luciferase signal amplification therefore it is extremely sensitive but tends to give high percentage of false positives. The first aim of the current project was to verify whether the top hit candidates are genuine MAPK interactors or potential substrates. This validations process was designed to take advantage of the nanoluciferase fragment complementation assay (NanoBit) which is capable for real-time monitoring of protein-protein interactions in a reversible manner in living cells [2] (**Figure 1.A**). In order to test a set of candidates the original Nanobit vectors were modified to be compatible with Gateway cloning technique allowing rapid generation of tagged fusion proteins and Western blot verification of proper expression levels.

The first target – ERK2 – has failed to produce detectable signal in pair with any of the candidates while the known ERK interactor RSK1 showed strong and reliable readout demonstrating valid assay parameters (**Figure 1.B**). In contrast, the interaction between p38α and CEP89, CERKL and KCNB1 has been verified but found to be relatively weak compared to a well-known p38 substrate, MK2, used as positive control. CEP89 is a centromere associated proteins with poorly discovered function but it could be connected to cell division and cytoskeletal remodeling while CERKL and KCNB1 have

important neuronal functions primarily [3, 4]. These results indicate that the mentioned proteins are not responsible for p38 modulation but rather could be weak substrates released after the phosphorylation event (**Figure 1.C**). Unexpectedly, JNK1 showed signals with POLR2J3, CEP89 and FBXO43 comparable to the applied negative control of the Nanobit system consequently failing to pass the verification of any of the predicted candidates (**Figure 1.D**).

These data led us to redesign the prediction concept and take advantage of the generated cell-lines in *chapter 1.2* to apply a transcriptomic approach to detect the MAPK fingerprint and to identify the responsible transcriptional regulators under MAPK control, see in *chapter 1.5*.

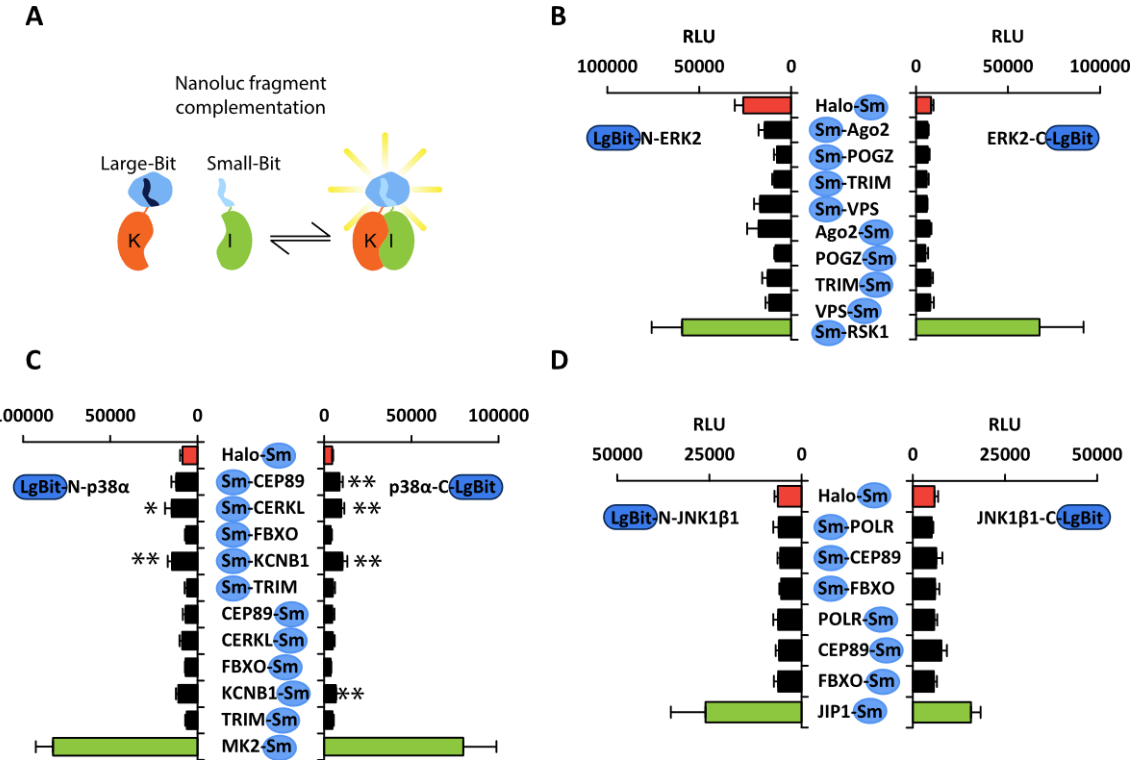

Figure 1. Summary of candidate validation experiments to identify novel MAPK interactors. A) Principle of Nanobit fragment complementation assay. **B)** Results of Nanobit assay on ERK2 and interactor candidates, RSK1 construct was used as positive interaction control. **C)** Results of Nanobit assay on p38α and interactor candidates, MK2 construct was used as positive interaction control. **D)** Results of Nanobit assay on JNK1 and interactor candidates, JIP1 construct was used as positive interaction control. LgBit: Large-Bit Nanoluc fragment, SmB: Small-Bit Nanoluc fragment, relative orientations are representing the N- or C-terminal fusions. Mean ± SD n = 4, **: $p < 0.01$, *: $p < 0.05$ *vs.* Halo-tag Small-bit fragment used as negative control using one-way ANOVA followed by Tukey *post hoc* test *vs.* Halo-tag.

1.2. Generation of genetically encoded inducible JNK activator construct

The testing of novel target phosphorylation (including interactors and adaptor-driver substrates) of MAPKs ERK, p38 and JNK in cellular environment required efficient temporal activity control of these kinases. This could be achieved by inducible expression of a constitutively active MAP2Ks (Tet-ON system). Previous studies predominantly used MAP2K phosphomimicing mutations replacing the need for upstream stimulation. Preliminary experiments determined that constitutive active MKK1 (S218E/S222E) and MKK6 (S207E/T211E) phosphorylates the respective MAPKs on a sufficient level, however the most commonly applied MKK7 (S271E/S275E) mutant had poor performance in the cell lines intended to be used. Considering that JNK had especially important and interesting targets this technical limitation had to be addressed first.

Taking advantage from the overlapping activation of JNKs by MKK4 and MKK7 we designed a thorough combined mutational screen to improve this specific MAPK activation capability (**Figure 2.A**). One possible explanation of the suboptimal MKK7 mutant performance could be the insufficient phosphomimicing negatively charged surface therefore the region of the replaced amino acids was extended incorporating glutamates/aspartates in the neighboring positions of the original phosphoserine and phosphothreonine residues in both MKK7 and parallelly in MKK4. The potential weaker substrate binding of MKK4 in combination with the suboptimal phosphomimicing mutation could also result insufficient downstream phosphorylation. To overcome this, we mutated the MKK4 D-motif replacing it with an improved one from a strong MAPK binding adapter, JIP1. However, these steps were still insufficient to achieve JNK activation comparable to non-specific strong activators like sorbitol or anisomycin (**Figure 2.B**, left panel). Speculating that the suboptimal MAPK binding could be the result of the atypical C-terminal lobe of MKK4 compared to other MAP2Ks, we redesigned this domain based on MKK6 having a potentially more preferable homologue region. Incorporating this third feature, however, was still incapable for the required JNK activation (**Figure 2.B**, right panel). Next, we returned to MKK7 and tried to improve its performance via *in situ* activation by the fusion of constitutively active, unregulated kinase domain from MAP3Ks. The MEKK3 kinase domain was extremely powerful resulting strong JNK induction, however the bystander activation of ERK and p38 was also observable consequently unsuitable for specific JNK-activation (**Figure 2.C, D** and **E**). In contrast, MLK3 kinase domain fusion resulted in rapid rise of active phosphorylated JNK and downstream cJUN and ATF2 activation while the non-targeted MAPKs remained unaffected (**Figure 2.C, D** and **E**).

The optimized JNK activation achieved via this part had supported parallel projects of the lab and already resulted two publications (*Kirsch et al. Nat Comm 2020*, *Singh et al. Int J Mol Sci 2022*).

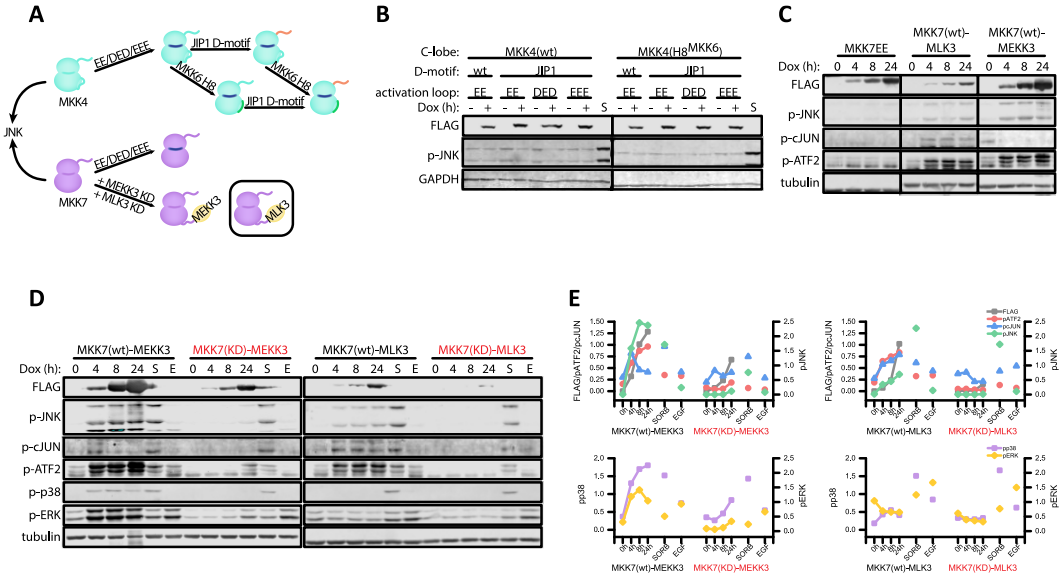

Figure 2. Systematic evolution of genetically encoded JNK activating constructs. A) Schematic representation of the applied mutations. **B)** Efforts to improve the human MKK4 JNK activation capability. Abbreviation of mutations: *EE*: *S257E/T261E*, *DED*: *S257D/T261E*, *EEE*: *S257E/T261E/D263E*; *JIP1* D-motif: MKK4 D-motif replacement with JIP1 D-motif, $H8^{wt}/H8^{MKK6}$: MKK4 C-lobe H8 helix is wild-type or replaced with corresponding region from MKK6 (*308-PKWNSV-313 → 308-DSWGTP-313*) **C)** Evaluation of JNK activating performance of MKK7 fused to MEKK3 or MLK3 kinase domains **D)** Analysis of background non-specific effects of MEKK3 or MLK3 via the fusion to kinase-inactive (KD) MKK7 **E)** Temporal resolution of downstream phosphorylation by MKK7-MEKK3 or MKK7-MLK3 constructs. MKK7 kinase dead (K149R) but active MEKK3/MLK3 kinase domain containing mutants were used as background control.

1.3. Adapter-mediated phosphorylation of JNK substrates

We applied bioinformatic screen to search for common interaction partners of MAPKs and MAPK targets that are unlikely to undergo canonical kinase-substrate docking in order to reveal adapter proteins facilitating the phosphorylation of these type of substrates. Three presumptive substrate-adapter pair have been selected to test whether JNK-mediated phosphorylation could be supported by target anchoring adapter proteins. The substrate candidates were selected based on connection to neuronal development and function as amyloid precursor protein (APP) and Sirtuin1 deacetylase (SIRT1). APP T668 phosphorylation was demonstrated to be involved in posttranslational processing, maturation and amyloid fragment generation via the cleavage of the full-length APP protein while S27 SIRT phosphorylation affects the its transcriptional regulator activity. Importantly, both sites were suggested to be under JNK regulation however direct evidences yet to be provided. To be able to control JNK activation and adapter expression in the same cells separately, a double inducible system has been designed and constructed using the previously established Tet-ON approach for MKK-MLK3 JNK activator (labelled as Dox) while adapter proteins were expressed under a similar but coumermycin-inducible system (labelled as Com) (**Figure 3.A**). This second system has been validated for this study and selected over similar small-drug activated techniques based on superior induction capability and low background, however it should be noted that coumermycin-driven expression still lags behind

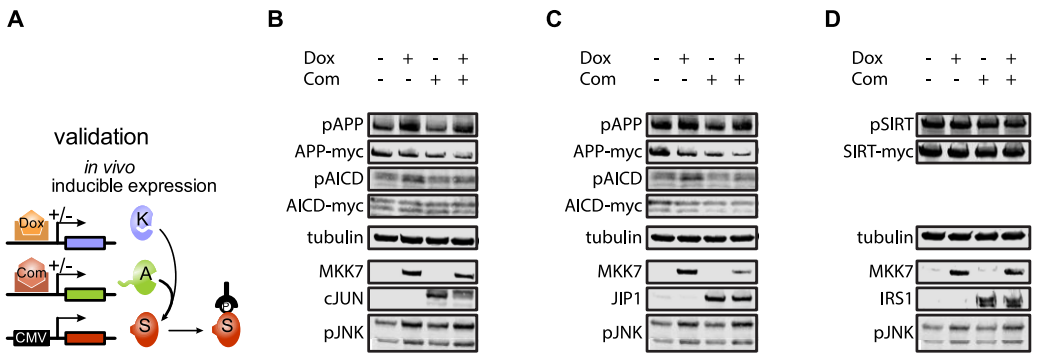

Figure 3. Evaluation of adapter-mediated phosphorylation of JNK substrates. A) Schematic summary of double-inducible system for adapter proteins and MAPK-activator MAP2K-based construct using Doxycycline and Coumermycin, respectively **B)** Western blot panel of cJUN as candidate adapter for APP protein. **C)** Western blot panel of JIP1 as presumptive adapter for APP protein. **D)** Western blot panel of IRS1 as adapter for SIRT1 protein.

doxycycline-based system in time-response curve and overall induction capacity. This information led us to the consideration to use doxycycline for MAPK activators to obtain sharp rise of MAPK phosphorylation and apply coumermycin for adapters where slower protein level build-up could be tolerated.

The JNK activation increased T668 APP phosphorylation in general providing the first direct evidence that physiological level of JNK has the capability to phosphorylate APP at this site in living cells. The increased presence of cJUN as adapter – JNK target itself – showed no significant effect on T668 APP phosphorylation (**Figure 3.B**). While JIP1 similarly lacked a modulatory effect on T668 APP phosphorylation a minor tendency for decreased stability of APP in presence of active JNK and JIP1 was observable (**Figure 3.C**). In contrast to the APP/JNK relationship the S27 phosphorylation of SIRT1 showed complete resistance to both JNK activation and coexpression of its substrate IRS1 demonstrated to undergo SIRT1-dependent deacetylation itself (**Figure 3.D**). These data indicates that SIRT1 is not regulated by JNK at this site however this phase of the present study drew our attention to the complex phosphorylation-dependent regulatory feedback of IRS1 that work will be elaborated in *chapter 1.4*.

It is important to note that APP undergoes series of proteolytic cleavage including amylogenic Aβ42 and non-amylogenic Aβ40 fragment generation while the C terminal part of the protein is released into the cytosol [5, 6]. This latter fragment includes the amyloid precursor protein intracellular domain (AICD) that is speculated to have transcriptional regulator activity [7]. In its posttranslational processing and theoretical function AICD highly resembles the NOTCH intracellular domain (NICD) fragment having verified transcriptional regulator activity however it is important to emphasize that AICD alone is unlikely to be able to bind DNA directly since it lacks any canonical DNA-binding motif. The generation and intracellular transport of AICD – despite its potential role in amyloid pathobiology – is poorly studied. The region of AICD includes the T668 site that raises the question whether it has an effect on AICD generation, nuclear transport and interaction network ultimately modulating its transcriptional regulatory potential. A relative increase of T668 phosphorylated AICD had been observed indicating that JNK might have a role in its generation and/or stability. Therefore, we performed quantitative Western blot experiments and detected increased phosphorylation on T668 site

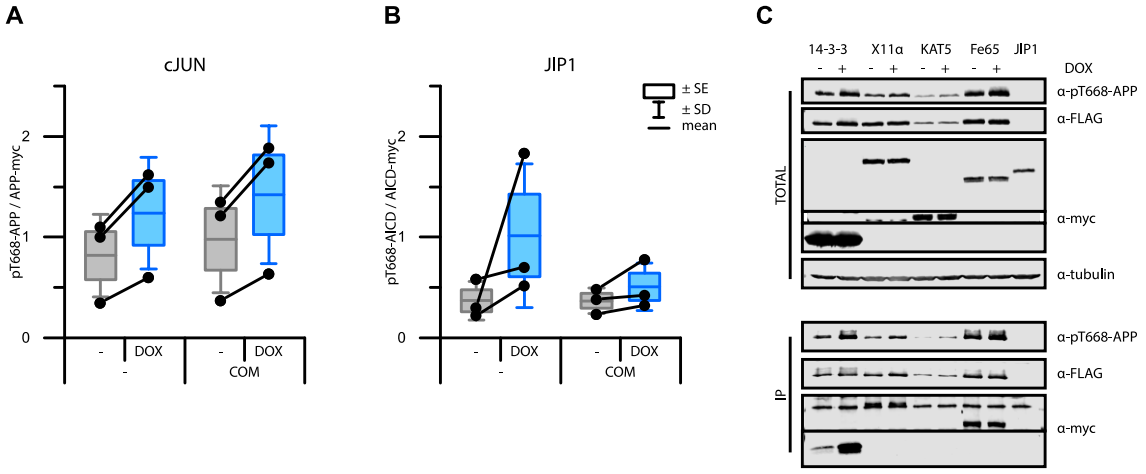

Figure 4. Quantitative analysis of AICD phosphorylation and mapping of APP/AICD cofactor interactions by JNK activation. A) Summary of quantitative Western blots to detect the relative phosphorylation of AICD fragments by JNK induction (DOX) and/or cJUN coexpression (COM). B) Summary of quantitative Western blots to detect the relative phosphorylation of AICD fragment by JNK induction (DOX) and/or JIP1 coexpression (COM). Co-immunoprecipitation experiments mapping the JNK-dependence of APP interaction with 14-3-3, X11α, KAT5, FE65 and JIP1 proteins.

by specific JNK activation and found it unaffected by the coexpression of cJUN or JIP1 indicating that the proposed adapters neither facilitate not inhibit the AICD production (**Figure 4.A** and **B**). Our next question targeted the downstream consequences of the T668 phosphorylation of APP, specifically whether its interactions with partners involved in AICD production are affected by JNK activity. Our data revealed an increased 14-3-3 binding by JNK-mediated phosphorylation indicating that the initial step of AICD production could be modulated by JNK but the adapters responsible for carrying AICD into the nucleus are resistant to T668 phosphorylation (**Figure 4.C**).

The previous findings led us to focus on the transcriptional activity of AICD and its connection to T668 JNK phosphorylation. Taking advantage of its similarity to NICD we used a luciferase reporter system consisting of Rbpj-binding sites and endogenous Rbpj-containing Hes1-promoter reported to be affected by AICD alongside its known regulation by NOTCH/NICD (**Figure 5.A**). The full-length APP protein did not affect the basal activity of the artificial Rbpj promoter construct nor it reacted to JNK activation (**Figure 5.B**). In contrast, Hes1 promoter was found to be induced by full-length APP protein in a JNK-dependent manner (**Figure 5.C**). Importantly, full-length APP protein was reported to require the sequential contribution of a multiprotein cofactor complex to be properly cleaved and transported to the nucleus [8] therefore even if JNK-mediated phosphorylation promotes/inhibits AICD generation or affects its stability it is unlikely to be sufficient to have an effect on the complete genomic actions of AICD. The required proteins for AICD import include Fe65 (APBB1), X11-Like (APBA2), 14-3-3 and KAT5 is speculated to be one of its transcriptional effectors as chromatin state regulator. We followed our study focusing on how these co-regulators are modulated by JNK activity. Without Fe65 and KAT5 the adapters JIP1 and 14-3-3 showed no effect on Hes1 promoter activity, however Fe65 and KAT5 in combination revealed an inducing effect for JIP1 while 14-3-3 was not indicated to modulate the process (**Figure 5.D**). Notably none of these effects were affected by JNK activation via the doxycycline-dependent induction system (**Figure 5.D**). These experiments proved that C-terminal fragment of APP protein has transcriptional regulator capability but the complex transport and cofactor apparatus – at

least – in HEK-293T cells can severely restrict its full potential. It is unclear whether the AICD cleavage from APP and nuclear import require the contribution of additional uncharacterized factors or the regulator potential of AICD is relatively weak needed to be amplified by more potent transcriptional modulators. Therefore, in the next set of experiments we removed the posttranslational processing as limiting factor expressing directly AICD fragments truncated at amino acid position of 652 or 639, the two sites found to be cleaved at most frequently. These data revealed the AICD carries the inherent potential to regulate both Rbpj-binding site containing promoters itself or via the contribution of cofactors on endogenous levels (**Figure 5.E** and **F**). This effect was found to be unaffected by JNK activity. The AICD fragment-dependent induction was detectable in the presence of Fe65, KAT5 and JIP1 but additive affect could not be observed indicating the primary importance of these proteins in the prenuclear processing of APP/AICD (**Figure 5.G**). Taken together these data with the previous set of experiments indicates a role for JNK in AICD production and/or stability however its downstream genomic actions are most likely independent from JNK. Our results also demonstrate that AICD is capable to act through a similar transcription factor binding site regions as reported for NICD.

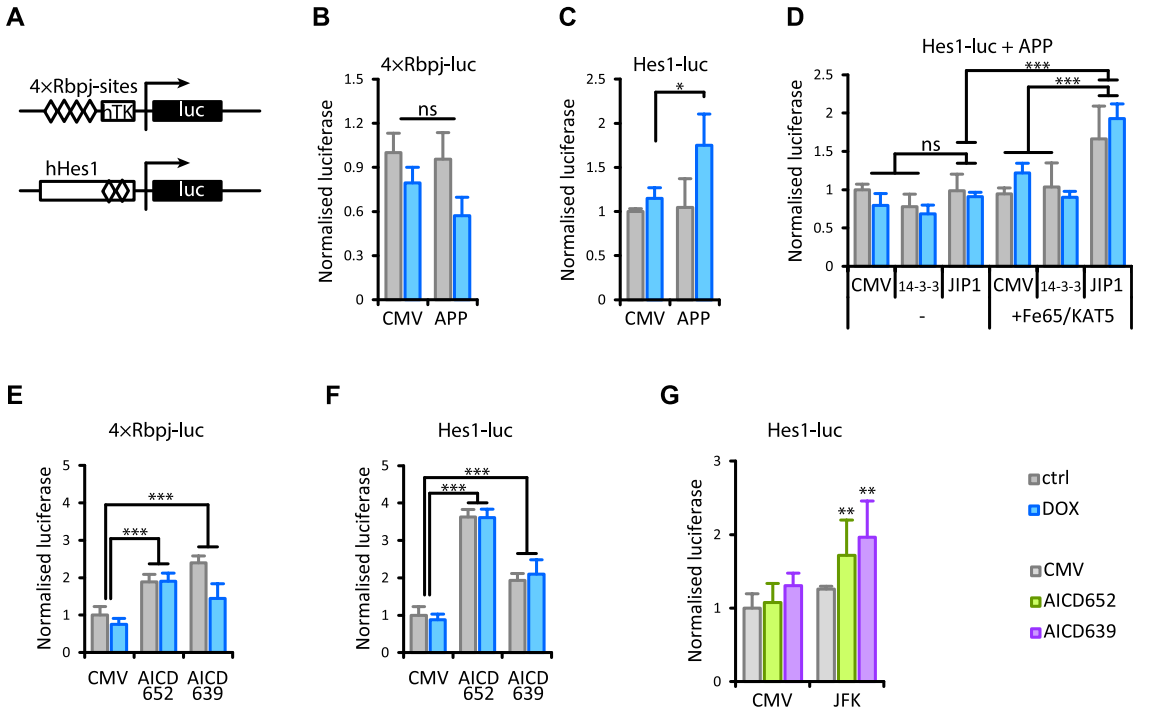

Figure 5. Importance of JNK in the genomic actions of APP/AICD. A) Schematic drawing of luciferase reporter constructs used in the experiments. **B)** Dual Luciferase measurements of *4×Rpbj-luc* cotransfected with full-length APP expression vector and inducible MKK7-MLK3 construct in HEK-293T cells. **C)** Dual Luciferase measurements of *Hes1-luc* cotransfected with full-length APP expression vector and inducible MKK7-MLK3 construct in HEK-293T cells. **D)** Dual Luciferase measurements of *Hes1-luc* and full-length APP cotransfected with Fe65/KAT5 cofactors and/or 14-3-3 or JIP1 adapters. **E)** Dual Luciferase measurements of *4×Rpbj-luc* cotransfected with AICD fragments. **F)** Dual Luciferase measurements of *4×Rpbj-luc* cotransfected with AICD fragments. **G)** Effect of Fe65/KAT5 and JIP1 (JFK) on ACID fragment-dependent induction of *Hes1-luc* reporter construct. Doxycycline was applied in 2 µg/ml final concentration after 24 hours of serum starvation. Mean ± SD n = 3, ***: $p < 0.001$, **: $p < 0.01$, *: $p < 0.05$ by two-way ANOVA followed by Tukey *post hoc* test.

1.4. Serine phosphorylation affects IRS1 activity via tyrosine dephosphorylation

The study of IRS1 as SIRT1 adapter for JNK-dependent S27 phosphorylation redirected our attention to tyrosine phosphorylation of IRS1 protein. IRS1 undergoes several phosphorylation events upon insulin or insulin-like growth factor stimulation that includes tyrosines in close proximity of serines. Its function in signaling is evoked through the phosphorylation of these tyrosines and rapidly deactivated via dephosphorylation by phosphatases like SHP2 that process is required to avoid receptor desensitization. Importantly, SHP2 binding is facilitated by phosphoserines and secondly, since serines in question are followed by prolines potentially that postulates the involvement of proline-directed kinases like MAPKs.

In order to test this hypothesis, we studied the insulin response of IRS1 phosphorylation by in the presence of serine-phosphorylation (wild-type) or when serines are replaced to non-phosphorylatable alanine (SA mutant, S616A/S632A/S666A/S736A). The basal tyrosine phosphorylation at Y612 site in IRS1 was found to be elevated in the mutant while its induced phosphorylation upon insulin treatment had a tendency to be increased but it failed to show a significant effect (**Figure 6.A** and **B**). The kinetic effect of insulin was, however, similar in both cases (**Figure 6.C**) and we did not find stimulatory effect of JNK activation (data not shown). These results indicate that the serine-dependent feedback on phosphotyrosines can modulate the sensitivity of insulin response through IRS1 that could have potential implications in the molecular pathology of insulin resistance. The study of IRS1 phosphorylation is submitted as manuscript and expected to be accepted in the third quarter of 2022 for publication (*Zeke et al. Nat Comm 2022*).

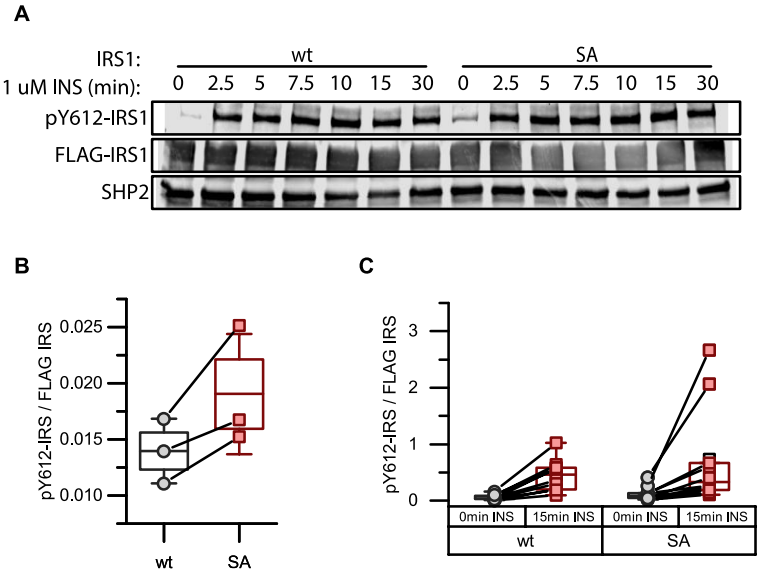

Figure 6. IRS1 serine phosphorylation regulates its tyrosine phosphorylation-dependent activation. A) Western blot demonstrates the kinetic effect of insulin stimulation in HEK-293T cells transfected with wild-type (wt) or serine-alanine (SA) mutant of IRS1 and phosphatase SHP2. **B)** Basal tyrosine phosphorylation of wt and SA mutant IRS1, n=3. **C)** Effect of 15 minutes of insulin stimulation on wt or SA mutant IRS1, n=10. Mean ± SEM ± SD.

1.5. Identification of MAPK-dependent transcriptional regulators

The first part of the project was predominantly concentrated on the identification of MAPK effectors and transcriptional regulators starting from the direct or indirect interactions to MAPKs moving toward genomic actions. This second phase reversed the strategy and took advantage of the obtained capabilities to achieve specific MAPK activation and use the alterations in transcriptome after the induction of a given MAPK as starting data to reconstruct the signaling network from the genomic effect upward. Therefore, cell lines were generated carrying Doxycycline-inducible constitutively active MAP2Ks to control JNK and p38 activity using lentiviral gene delivery. The applied cell lines included fundamentally different in origin as neuronal SH-SY5Y, endothelial Eahy926 and hepatic HepG2 (**Figure 7.A**). Using the previously established genetically encoded inducible MAPK activation system specific MAPK phosphorylation has been successfully achieved (**Figure 7.B**).

Samples from inducible SH-SY5Y MKK6EE / SH-SY5Y MKK7ACT / SH-SY5Y double MKK6EE+MKK7ACT / EAhy926 MKK7ACT / HepG2 MKK7ACT were treated with Doxycycline for 0-, 2- and 6-hours and processed for RNAseq analysis. Differential gene expression was considered at a minimum of 2-fold change normalized counts and $p_{adjusted}$ of 0.05 excluding genes blacklisted from MKK7KD and MKK6KD (kinase-dead) samples. First, the SH-SY5Y cell lines were compared. 2-hours of induction was chosen to detect directly affected genes by the MAPKs however were proven to be insufficient to obtain relevant data. In contrast, in the 6-hour groups we observed remarkable difference between JNK and p38 activation: JNK induction resulted significantly more affected genes (**Figure 8.A**

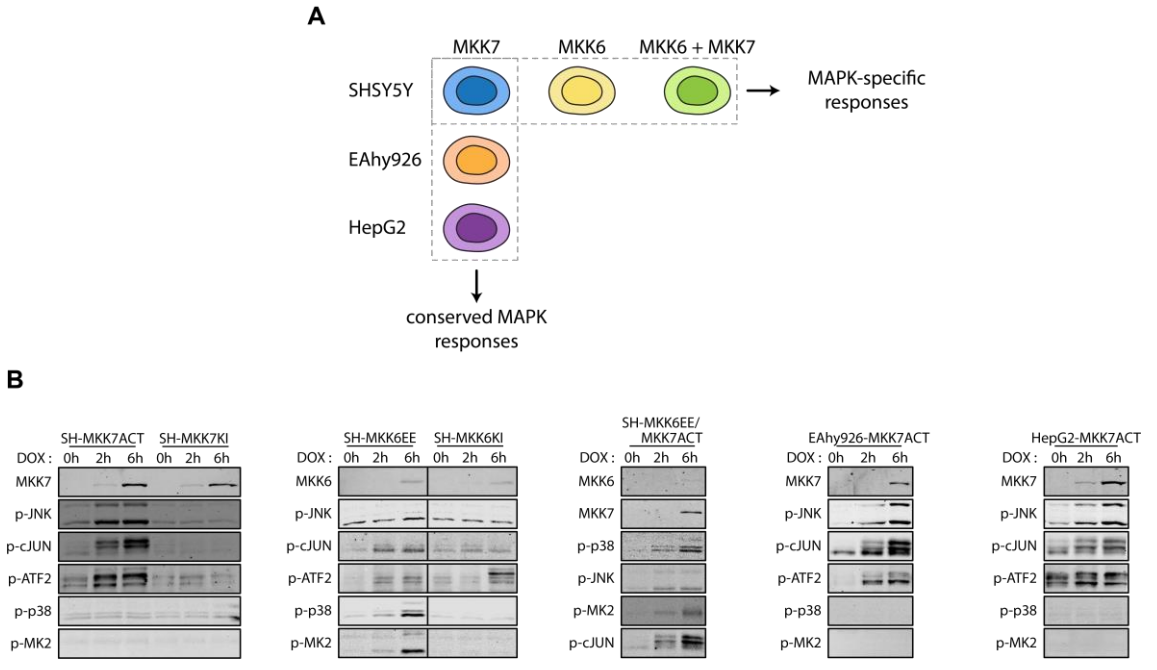

Figure 7. Generation of inducible MAPK activatable cell lines. A) Concept of the study and design of cell lines carrying inducible MAPK activator constructs. **B)** Western blot demonstration of efficient and specific activation of selected MAPKs and MAPK substrates in the genetically engineered cell lines.

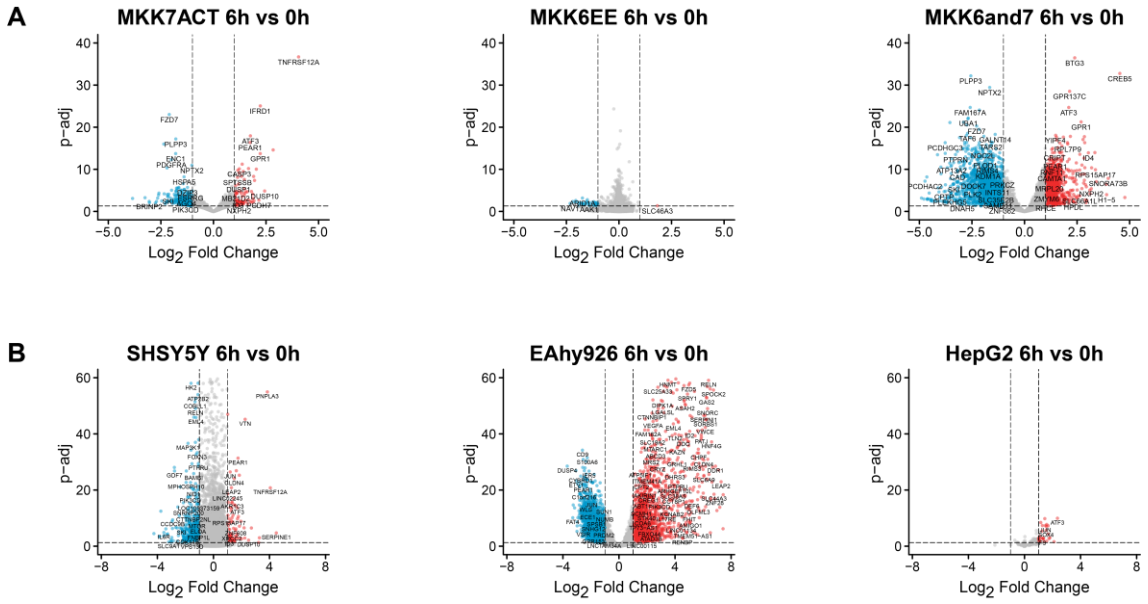

Figure 8. Volcano-plot of the differentially expressed genes. A) Comparison of SH-SY5Y cell lines expressing MKK7ACT or MKK6EE separately or coexpressing both transgene constructs. Cells were treated for 6-hours with 3 µg/ml Doxycycline vs control. **B)** Comparison of MKK7ACT expressing SH-SY5Y, EAhy926 and HepG2 cell lines treated with 3 µg/ml Doxycycline for 6-hours vs control. Genes with fold change = 2 and $p_{adjusted} < 0.05$ are highlighted.

left and middle panel). The most notable effect was the additivity of JNK and p38 resulting one order of magnitude higher differentially expressed genes compared to the single activation of JNK or p38 (**Figure 8.A** right panel).

Next, starting from the differential expression dataset we aimed to identify transcription factors potentially responsible for the observed transcriptomic responses. Two strategies were applied. First, using hierarchical clustering, the genes with similar temporal expression profile were analyzed together by the application of HOMER (Hypergeometric Optimization of Motif EnRichment) algorithm looking for known transcription factor binding sites and enriched sequences indicating potential *de novo* regulators. The second method focused on the unique and coregulated genes among separate cell lines. In case of the three SH-SY5Y cell lines we defined three major clusters, one is primarily under the potential regulation of well-known JNK-dependent factors like ATFs, CREB5 and NFILs (**Figure 9.A**). Notably, the second group, consisting another one-third of the genes had Mef2a and Mef2b sites those are mostly known to be p38-dependent. Interesting to note that despite not having significant number of differentially expressed genes in case of the SH-SY5Y MKK6EE cell line the fingerprint of p38 could still be traced through temporal expression profiles within a cluster. The third cluster did not show identified transcription factor binding sites however novel overrepresented sequences in close proximity to transcription start sites were revealed (**Figure 9.A**). Grouping the upregulated genes based on cell-line dependent differential expression profile demonstrated JNK dominance in case of coactivation of both p38 and JNK (C-JUN ATF2 and CRE have been also predicted for the MKKACT and the double cell line, **Figure 9.B**). The coactivation of p38 and JNK suppressed genes under regulation of factors like Octs and KLFs, known to promote self-renewal capacity and pluripotency indicating that these two MAPKs can contribute to have a negative effect on this cell fate determination, at least in neuronal transcription factor milieu.

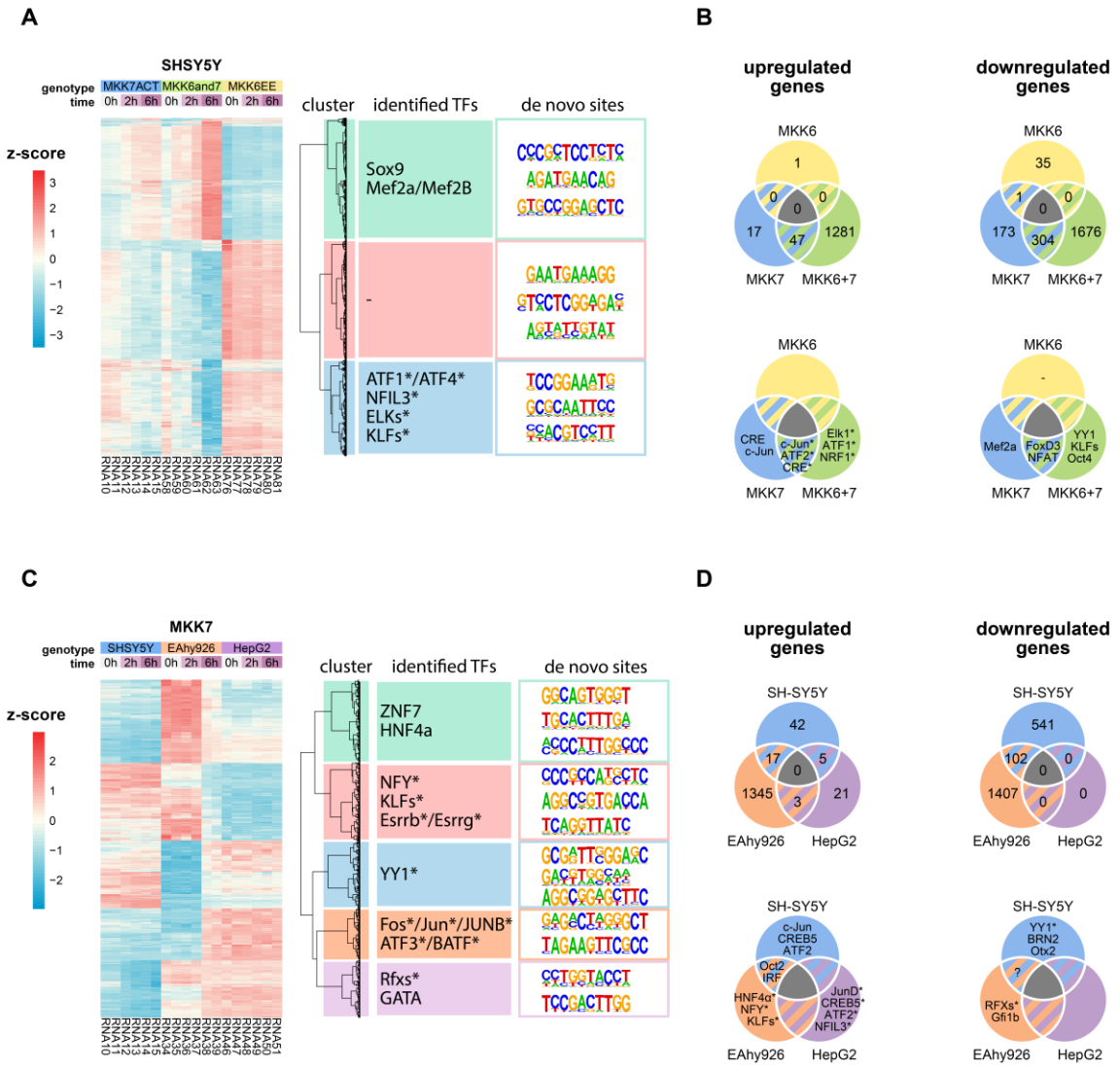

Figure 9. Summary differentially expression and cluster analysis and predicted transcription factors from RNAseq analysis of MAPK activation in cell lines with different origin. A) Heatmap and hierarchical clustering of genes from SH-SY5Y MKK6/MKK7 and MKK6+MKK7 double cell lines followed by transcription factor binding site analysis using HOMER algorithm. **B)** Transcription factor binding site prediction in the SH-SY5Y MKK6/MKK7 and MKK6+MKK7 double cell lines. **C)** Heatmap and hierarchical clustering of genes in SH-SY5Y, EAhy926 and HepG2 MKK7 cell lines followed by transcription factor binding site analysis using HOMER algorithm. **D)** Transcription factor binding site prediction in the SH-SY5Y, EAhy926 and HepG2 MKK7cell lines.

Comparing the same MAPK, JNK, in three different cell lines as background revealed a fundamental difference how the already presented transcriptional regulatory network can modify the outcome of the same given signal. Using cluster analysis, we identified 5 closely regulated groups of genes, including one predominantly under canonical JNK effector factors like Fos, Jun and ATFs (**Figure 9.C**). The remaining four clusters are dominated by transcriptional factors less connected to JNK, including HNFa, KLFs Essrb/Essrg and Rfxs. These data provide a starting point to understand how JNK activation is diversified in different cellular environments and can be finetuned to cell-specific expressional changes. The results also revealed common enriched sequences in gene promoter regions to be connected to recently unknown transcriptional regulators under direct or indirect JNK regulation. Another interesting difference has been found in the transcription factors predicted to be responsible for cell line-specific alterations. While HOMER screen identified canonical JNK-dependent factors like Jun, ATF2, CREB5 for SH-SY5Y and HepG2, EAhy926 showed remarkably different transcriptional factor profile, less explored to be controlled by JNK as HNF4a, NFY and several KLFs (**Figure 9.D**).

In the following part of the analysis, we moved from direct DNA binding factors to focus on major cellular pathway alternatively regulated by MAPK activation to connect the uncovered regulators to functional consequences. Therefore, we applied several bioinformatic methods based on somewhat different principle to identify differentially regulated signaling networks. The most promising results came from gene set enrichment analysis (GSEA) which is not restricted to differential expression but uses ranked genes from each sample consequently complementing the results of transcription factors analysis and those separate approaches could be connected after.

The comparison of MKK6 and MKK7 SH-SY5Y cell lines verified an additive effect of the two MAPKs primarily upregulating oxidative metabolism-related pathways. As a notable difference, while MKK7/JNK stimulated UV-responsive genes and TNFα signaling, MKK6/p38 induced MTORC, common regulator hub for several signals controlling cellular and systemic metabolism. Similar effect could be observed in case of the suppressed pathways, the two MAPKs primarily inhibited morphology-related signals like Hedgehog and Wnt, while p38 induction had additional effect on estrogen- and TGFβ-related genes. In the neuronal SH-SY5Y cell line, the two MAPKs negatively affected cell cycle regulation potentially indicating the known promotion of apoptotic processes (**Figure 10.A**).

Rather revealing results came from the analysis of MKK7/JNK in the three cell lines on different origin. In accordance with the transcription factor binding site prediction analysis, our data indicate that despite having common core transcription factor pool that transmits transcriptional effects, as seen previously, the outcome of the activation is remarkably different. Interestingly, the neuronal SH-SY5Y and endothelial EAhy926 cell lines showed remarkable overlapping activation and suppression of pathways while the hepatic HepG2 responded with a fundamentally selective pattern. (**Figure 10.B**).

Currently, the results from the transcriptomic analysis of MAPK-dependent actions are arranged to prepare the manuscript and expected to be submitted later this year.

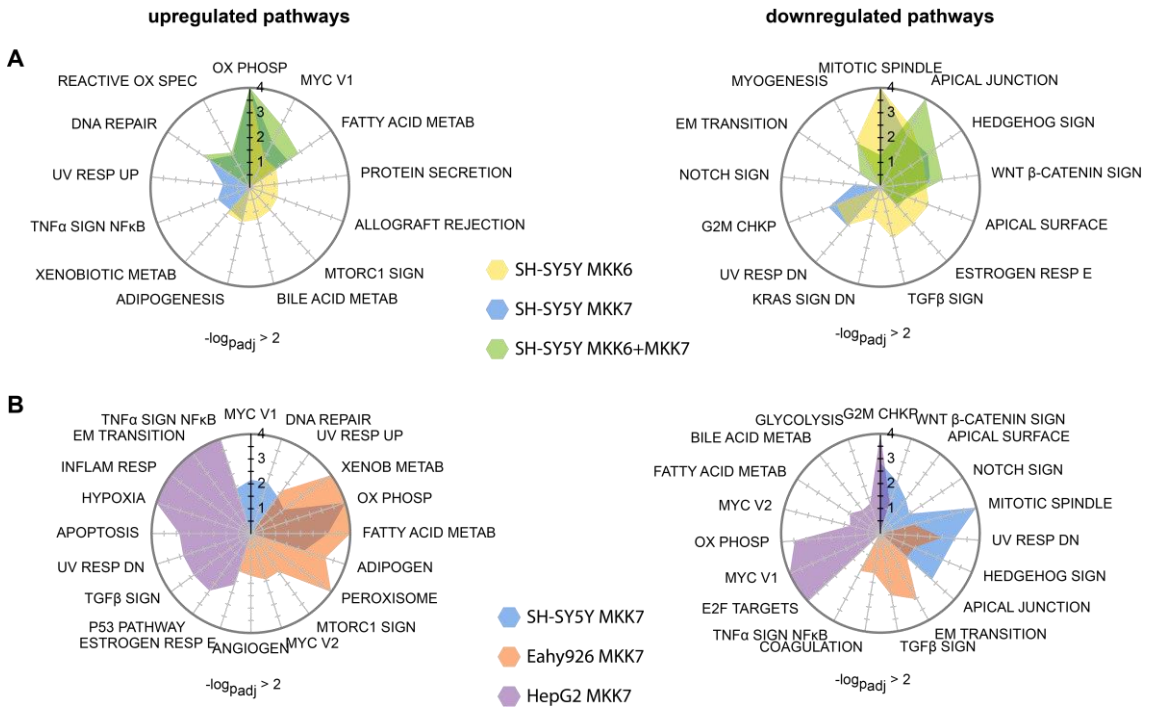

Figure 10. Summary of GSEA analysis of RNAseq dataset after 6-hours of MAPK activation in SH-SY5Y, EAhy926 and HepG2 cell lines. A) Significantly altered hallmarks have been depicted from GSEA analysis on gene sets from SH-SY5Y MKK6/MKK7 and MKK6+MKK7 double cell lines. **A)** Significantly altered hallmarks have been depicted from GSEA analysis on gene sets from SH-SY5Y, EAhy926 and HepG2 MKK7 cell lines.

3. Summary

We aimed the better understanding how MAPK signals transmitted toward the genome via extending MAPK signaling network from two directions: identifying novel interactors and by transcriptional responses evoked by specific MAPKs. We verified novel p38 targets primarily connected to cytoskeletal and neuronal regulation. Our data demonstrated the JNK phosphorylation of amyloid precursor protein (APP) can alter its role in transcriptional regulation via affecting its posttranslational processing. We proved the phosphoserine-dependent phosphotyrosine dephosphorylation of IRS1 protein which can counteract a potential receptor desensitization response in insulin signaling. In RNAseq studies we targeted MAPK-specific genomic actions applying genetically modified cell-lines for specific MAPK activation. We found that the activation of a single MAPK – that is usually not the case using agonists – results in a moderate response by the transcriptome however a combined induction has a surprising additive effect. It could be speculated whether the interconnected activation and downstream effects of different MAPKs are required for efficient signal transduction. We also revealed that the activation of a single MAPK, namely JNK, can result in fundamentally different responses based on cell origin indicating that MAPK signaling should be considered well-integrated within cell-specific transcriptional regulatory systems.

4. References

1. Eyckerman, S., et al., *Design and application of a cytokine-receptor-based interaction trap*. Nat Cell Biol, 2001. **3**(12): p. 1114-9.
2. Dixon, A.S., et al., *NanoLuc Complementation Reporter Optimized for Accurate Measurement of Protein Interactions in Cells.* ACS Chem Biol, 2016. **11**(2): p. 400-8.
3. Yu, S., et al., *CERKL gene knockout disturbs photoreceptor outer segment phagocytosis and causes rod-cone dystrophy in zebrafish.* Hum Mol Genet, 2017. **26**(12): p. 2335-2345.
4. de Kovel, C.G.F., et al., *Neurodevelopmental Disorders Caused by De Novo Variants in KCNB1 Genotypes and Phenotypes.* JAMA Neurol, 2017. **74**(10): p. 1228-1236.
5. Pardossi-Piquard, R. and F. Checler, *The physiology of the beta-amyloid precursor protein intracellular domain AICD.* J Neurochem, 2012. **120 Suppl 1**: p. 109-24.
6. Bukhari, H., et al., *Small things matter: Implications of APP intracellular domain AICD nuclear signaling in the progression and pathogenesis of Alzheimer's disease.* Prog Neurobiol, 2017. **156**: p. 189-213.
7. Chen, Z.C., et al., *Phosphorylation of amyloid precursor protein by mutant LRRK2 promotes AICD activity and neurotoxicity in Parkinson's disease.* Sci Signal, 2017. **10**(488).
8. Sumioka, A., et al., *Role of 14-3-3gamma in FE65-dependent gene transactivation mediated by the amyloid beta-protein precursor cytoplasmic fragment.* J Biol Chem, 2005. **280**(51): p. 42364-74.